Condensational Growth of Drops Formed on Giant Sea-Salt Aerosol Particles

JØRGEN B. JENSEN AND ALISON D. NUGENT

Earth Observing Laboratory, National Center for Atmospheric Research,[a] *Boulder, Colorado*

ABSTRACT

The most basic aspect of cloud formation is condensational growth onto cloud condensation nuclei (CCN). As such, condensational growth of cloud drops is often assumed to be a well-understood process described by the drop growth equation. When this process is represented in models, CCN activate into cloud drops at cloud base, and it is often assumed that drops consist of pure water or that the hygroscopic contribution after drop activation is small because of the inclusion of only small CCN. Drop growth rate in adiabatic ascent in such models is proportional to supersaturation and assumed to be inversely proportional to the drop radius, thereby making the drop spectrum narrow with altitude. However, the present study demonstrates that drop growth on giant sea-salt aerosol particles (GCCN; dry radius $r_d > 0.5\,\mu m$) behaves differently. For typical marine stratocumulus updrafts and for drops grown on GCCN with sizes $r_d \gtrsim 2\,\mu m$, these drops typically remain concentrated salt solutions. Because of this, their condensational growth is accelerated, and they rapidly attain precipitation drop sizes through condensation only. Additionally, drops formed on GCCN may also grow by condensation in cloudy downdrafts. The strong effect of condensation on GCCN is important when carried through to calculating rain-rate contribution as a function of aerosol size. GCCN larger than $2\,\mu m$ account for most of the rainfall rate in the modeled precipitating marine stratocumulus.

1. Introduction

Clouds and aerosols have major impacts on climate (IPCC 2013). Marine boundary layer clouds in particular, including marine stratocumulus, cover about 22% of the ocean surface (Eastman et al. 2011) and play a key role in climate. Aerosols affect cloud albedo through the concentration of activated cloud drops (Twomey 1977), and aerosols affect a cloud's ability to develop precipitation and therefore the lifetime of the cloud (Albrecht 1989). Model parameterizations of the development of clouds are an integral part of climate models, and many observational studies of marine stratocumulus are based on the fact that models struggle to represent them accurately (e.g., Wood et al. 2011).

Much of the emphasis on understanding precipitation formation in marine stratocumulus and other warm clouds (no ice phase) has been on coalescence between cloud drops, notably gravitational stochastic coalescence (Telford 1955; Tzivion et al. 1987; Jensen and Lee 2008; etc.), turbulent entrainment (Baker and Latham 1979; Jonas 1996), turbulent enhancement to gravitational coalescence (e.g., Franklin et al. 2005; Wang et al. 2006), and radiative effects (e.g., Roach 1976; Lebo et al. 2008). In contrast, the condensation process leading up to the onset of coalescence has been accepted as being reasonably well described Pruppacher and Klett (1997), at least in the absence of entrainment (e.g., Baker and Latham 1979). Yet, in this manuscript we argue that many cloud process models and climate models miss important aspects of condensation in marine stratocumulus and, in part because of this, have inaccuracies in marine stratocumulus properties that can have further impacts on calculations of Earth's radiative balance. Microphysical parameterizations usually include condensation on small aerosol particles called cloud condensation nuclei (CCN). These particles are typical accumulation-mode particles and consist of sulfates and some sea salt (Gras and Ayers 1983) and an

---

ⓐ Denotes content that is immediately available upon publication as open access.

Corresponding author e-mail: Jørgen B. Jensen, jbj@ucar.edu

organic contribution (Novakov and Penner 1993). However, studies frequently omit condensation on giant sea-salt aerosol particles, also known as giant cloud condensation nuclei (GCCN) (all used interchangeably), here defined as having a dry radius $r_d > 0.5 \, \mu$m. If cloud and climate models include GCCN, this is often done only at cloud base (e.g., Fountikis and Nenes 2005, coarse mode aerosol) during the cloud droplet activation process. Many cloud models and cloud parameterizations omit consideration of the solute effect of GCCN particles on drop growth throughout the entire cloud (e.g., Lin et al. 1983; Feingold et al. 1999; Khairoutdinov and Kogan 1999, 2000; Morrison et al. 2005; Liu et al. 2006; Thompson and Eidhammer 2014). Some studies that do include the solute effect of GCCN through the entire cloud lifetime are Johnson (1982), Cooper et al. (1997), Blyth et al. (2003), Lasher-Trapp et al. (2005), Jensen and Lee (2008), Magaritz et al. (2009), Lowenstein et al. (2010), and Cooper et al. (2013). Additionally, there is a family of models like that of Shima et al. (2009) that calculate detailed condensational growth in a probabilistic sense.

Giant sea-salt particles, formed by breaking waves, are a ubiquitous part of the aerosol population in marine regions. The concentration and sizes of giant sea-salt aerosol particles vary as a function of wind speed (Woodcock 1953; see also the review in Lewis and Schwartz 2004). In the late 1950s, Mordy (1959) followed on a study of condensational growth by Howell (1949) by including giant sea-salt aerosols as part of the aerosol population. Mordy (1959) states clearly that, in condensational growth on sea-salt aerosols, larger particles grow more rapidly. The important impact of giant sea-salt aerosol particles in condensational growth and warm cloud formation has been known for decades, yet even today they are not often included in microphysical parameterizations in models. While condensational growth is reasonably well understood, we will argue that common simplifications to the growth of drops formed on GCCN particles result in an underestimation of their importance for warm rain formation. Among omissions is the importance of considering cloud drops formed on GCCN as concentrated, not dilute, salt solutions. To demonstrate this, we will reexamine the drop growth equation and the common simplifications used in implementing it into models.

The ability to understand the development of warm clouds and the formation of warm rain in a numerical model is a multifaceted problem. It requires the ability to capture aspects of cloud dynamics, including updraft strength, cloud-top height, turbulence, and collision and coalescence. Here, we take a narrow view of the problem by mostly focusing on the microphysical aspect of condensational growth in warm marine clouds. We do so by prescribing the dynamical aspects of a cloud in a simple theoretical model to measure changes in drop sizes activated on both accumulation-mode and giant sea-salt aerosols. We recognize that other approaches are equally valid but here choose to take a narrow view of the problem by focusing on the role of condensational growth onto both small CCN and larger GCCN. While the issue of condensational growth and the ability of giant nuclei to generate drizzle-sized drops has been studied in the past [Howell (1949) and Mordy (1959), among others], our approach and perspective is unique and sheds new light on an age-old problem that still exists today.

In the following manuscript, methods are included in section 2. This includes a description of the drop growth equation and model in section 2a and an overview of CCN and GCCN distributions used in section 2b. Results of a simple adiabatic parcel model used to calculate drop growth are covered in section 3a for stratocumulus and in section 3b for cumulus clouds, in both cases with a limited number of accumulation-mode aerosol and GCCN scenarios. Details of supersaturation and accelerated drop growth on GCCN are described in section 4, and the pure water hypothesis after drop activation is explored in section 5. An analysis of precipitation formation is conducted in section 6 to quantify the importance of GCCN when gravitational coalescence is included and to investigate which aerosol sizes are responsible for most of the rain rate. Finally, a discussion is in section 7, and a summary is in section 8.

2. Methods

a. Drop growth equations

The condensational growth of a cloud drop is described by the drop growth equation: that is (Grabowski et al. 2011),

$$\frac{dr}{dt} = \frac{1}{r} \frac{S - \exp\left[\dfrac{2\sigma_w}{R_v \rho_w T r} - \dfrac{3\mathscr{V}\Phi_s m_s M_w}{4\pi\rho_w M_s (r^3 - r_d^3)}\right]}{\dfrac{\rho_w R_v T}{e_s D} + \dfrac{\rho_w L_v}{KT}\left(\dfrac{L_v}{R_v T} - 1\right)}, \quad (1)$$

where r is cloud drop radius, r_d is the dry aerosol radius, S is the saturation ratio (e/e_s), and the rest of the variables are given in a symbol list in appendix A.

The first term in the numerator parentheses is the surface tension term, which is mainly important for very small drops (typically $r \ll 1 \, \mu$m). The second term in the numerator parentheses is the solute term; this term

is a key focus of this paper. In particular, the ratio of salt mass to volume of water in a drop, $m_s/(r^3 - r_d^3)$ in Eq. (1), is much larger for drops formed on GCCN than for drops formed on small CCN, even as the GCCN drops grow very large by condensation.

Andrejczuk et al. (2008) and Grabowski et al. (2011) have defined the equilibrium saturation ratio S_{eq} (when dr/dt is zero), which we give here in the following form:

$$S_{eq} = \exp\left[\frac{2\sigma_w}{R_v\rho_w Tr} - \frac{3\mathscr{V}\Phi_s m_s M_w}{4\pi\rho_w M_s(r^3 - r_d^3)}\right]. \quad (2)$$

Thus, the growth of a drop is proportional to an effective drop saturation ratio S_{eff}, here defined as

$$S_{eff} = S - S_{eq}. \quad (3)$$

For 1) highly dilute drops ($r \gg r_d$), 2) letting the inverse of the denominator of the second term in Eq. (1) be expressed as G (only a slowly varying function of drop size), and 3) doing a Taylor series expansion of the exponential function (keeping only the first two terms), simplifies Eq. (1) to the following:

$$\frac{dr}{dt} = \frac{G}{r}\left(S - 1 - \frac{2\sigma_w}{R_v\rho_w Tr} + \frac{3\mathscr{V}\Phi_s m_s M_w}{4\pi\rho_w M_s r^3}\right). \quad (4)$$

This equation may be further rewritten to be in a form similar to, for example, that of Rogers and Yau (1989):

$$\frac{dr}{dt} = \frac{G}{r}\left(S - 1 - \frac{a}{r} + \frac{b}{r^3}\right), \quad (5)$$

where a and b are parts of the drop surface term and drop solute term, respectively.

In contrast to the above, models that assume drop size distribution shapes come with their own host of assumptions and consequences (e.g., gamma distributions, typically with determined breadth that do not allow for natural development of the distribution tail), and such models typically assume that drops consist of pure water and that the surface term can be neglected; thus, the drop growth equation is further simplified to the following:

$$\frac{dr}{dt} = \frac{G}{r}(S - 1). \quad (6)$$

The assumption of highly dilute drops is a particular concern for marine clouds. During moderate wind conditions, marine clouds form in air with GCCN of sizes up to $r_d \approx 10\,\mu m$ (Woodcock 1953; Jensen and Lee 2008), a substantial mass of salt that impacts drop growth.

In the remainder of the present study, we use a version of the Jensen and Lee (2008) adiabatic parcel

model for calculation of condensational drop growth described in its complete form in appendix B. This model has predictive equations for drop radius r, water vapor mixing ratio q_v, temperature T, air density ρ_a, and altitude z. The model pressure is diagnosed using the hydrostatic equation, and total water mixing ratio q_t and moist static energy H are conserved. Additionally, we use the drop growth equation in the full form [Eq. (1)], as well as in some sensitivity study cases omitting the solute term, thus effectively assuming pure water drops. The model does not include radiation, sedimentation of particles, nor turbulent enhancement to coalescence; these limitations will be further considered in the discussion in section 7. As our main focus is on comparing drop growth rates, we specify simple kinematic parcel trajectories, usually consisting of an updraft followed by a downdraft, both with constant speeds. Because these values differ in various sensitivity tests, these values will be given in their corresponding section.

Mordy (1959) was a pioneer in cloud modeling with giant sea-salt aerosols and drop growth. We build on the work of Mordy (1959) in the following ways:

1) Mordy (1959) begins calculating drop growth at a relative humidity of 99% or larger, whereas we initialize drop growth much earlier at a RH of 86%: that is, well below cloud base.
2) Mordy (1959) only considers an updraft, whereas we consider both updrafts and downdrafts.
3) We use the equilibrium saturation ratio S_{eq}, as stated in Eq. (2); in a similar equation, Mordy (1959) makes the following approximations [see his Eq. (2)]:
   (i) the term in $\exp(\ldots)$ in our Eq. (2) is near unity, such that a Taylor series expansion (retaining only the first two terms) can be used for simplicity,
   (ii) drops are dilute, and
   (iii) the solute effect can be described by a constant van't Hoff factor ($i = 2$):

$$S_{eq} = 1 + \frac{2\sigma_w}{R_v\rho_w Tr} - \frac{3im_s M_w}{4\pi\rho_w M_s r^3}. \quad (7)$$

In contrast to approximations 3(i)–3(iii), we retain in our Eq. (2) the full exponential function, we treat the solute effect as $m_s/(r^3 - r_d^3)$, where Mordy (1959) uses m_s/r^3, and we allow for a full chemical potential formulation for NaCl-containing drops. Finally,

4) Mordy (1959) includes drop ventilation, whereas we do not include this in the drop growth equation, as it is not important for drops smaller than $60\,\mu m$ (Keith and Arons 1954).

TABLE 1. Submicrometer aerosol distributions, modified polluted and pristine, each consisting of two lognormal distributions, each with total number concentration N_a, geometric mean dry radius r_{dg}, and geometric standard deviation σ_g, based on Grabowski et al. (2011). Aerosols were defined in 100 bins covering the size range 0.01–0.5-μm dry radius (equivalent to 0.02–1-μm dry diameter, thus submicrometer), and all aerosols are assumed to be NaCl. The modified polluted aerosol concentration was reduced by 70% relative to the polluted aerosol concentration (Grabowski et al. 2011, their Table 5), while the pristine values remain unchanged.

	Modified polluted			Pristine		
	N_a (cm^{-3})	r_{dg} (μm)	σ_g	N_a (cm^{-3})	r_{dg} (μm)	σ_g
Mode 1	48	0.029	1.36	125	0.011	1.20
Mode 2	114	0.071	1.57	65	0.06	1.70

b. CCN and GCCN

Cloud drops in the adiabatic parcel model rely on an initial distribution of aerosols to act as cloud condensation nuclei. The primary aerosol distribution, based on Grabowski et al. (2011), is listed as the "modified polluted" case in Table 1 and as shown in Fig. 1. It consists of two lognormal modes, discretized into 100 bins covering 0.010–0.5-μm dry radius. The aerosol concentration has been reduced by 70%, hence the name "modified polluted," to better match the average drop concentration of about 150 cm^{-3} in the 2008 Variability of the American Monsoon Systems (VAMOS) Ocean–Cloud–Atmosphere–Land Study (VOCALS) project NSF/NCAR C-130 aircraft soundings through the depth of about 80 clouds. For a description of the VOCALS project, see Wood et al. (2011), and, for VOCALS aerosol observations, see, for example, Blot et al. (2013) and Twohy et al. (2013). Other model conditions are shown in Table 2. Note that larger GCCN with typical residence times of some hours are mostly generated locally in the VOCALS region, whereas smaller CCN and GCCN with residence times of days may also be generated externally to the VOCALS region and advected into the study area.

Multiple sensitivity tests are performed that include varying combinations of accumulation-mode aerosol distributions and GCCN. In addition to the modified polluted aerosol distribution, we use the "pristine" aerosol distribution (see Table 1) from Grabowski et al. (2011) to investigate drop growth in clean atmospheric conditions. Given that marine boundary layer clouds frequently occur over regions of breaking ocean waves, we augment the previously used submicrometer aerosol size distribution in some sensitivity tests with an observed size distribution of GCCN particles.
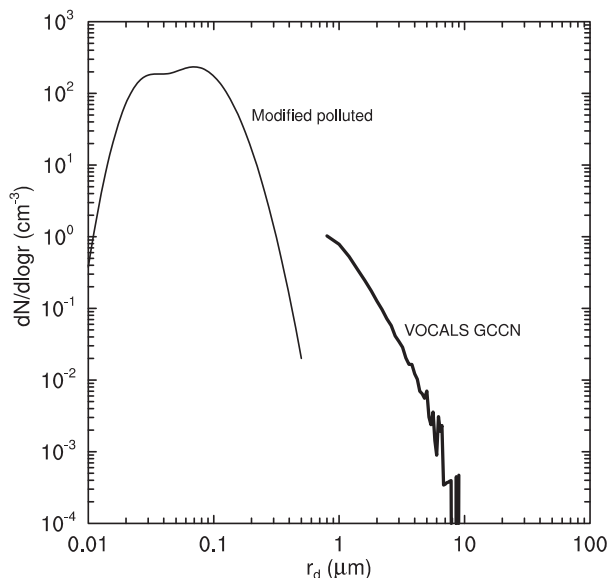

FIG. 1. Concentration spectrum of assumed size distribution for accumulation-mode aerosol particles, based on the modified polluted two-mode lognormal spectrum given in Table 1 and the GCCN measured from the NSF/NCAR C-130 on 18 Oct 2008 during the VOCALS deployment given in Table 3.

Some prior studies have used particle probe observations of solution drops below cloud base (e.g., Lasher-Trapp et al. 2002; Reiche and Lasher-Trapp 2010), but purely optical measurements using scattering probes may be affected by Mie uncertainty at small sizes or by sample volume uncertainty in the case of optical array probes. By contrast, in VOCALS we directly impacted GCCN particles onto polycarbonate microscope slides using the Giant Nucleus Impactor (GNI) and subsequent laboratory analysis. The slides were exposed at an altitude of 140 m (several hundred meters below cloud base) in the free airstream outside the NSF/NCAR C-130 during the 2008 VOCALS deployment over the southeast Pacific

TABLE 2. Model conditions for the drop growth model.

|	
Initial pressure (hPa)	938.5
Initial temperature (K)	284.3
Initial dewpoint temperature (K)	282.01
Initial saturation ratio	0.8561
Initial altitude (m)	600
Cloud-base pressure (hPa)	906.5
Cloud-base temperature (K)	281.5
Cloud-base altitude (m)	887.6
Stratocumulus cloud depth (m)	300
Updraft (m s^{-1})	0.4
Initial pressure (hPa)	938.5
Downdraft (m s^{-1})	−0.4
Cumulus cloud depth (m)	1500
Updraft (m s^{-1})	2.0
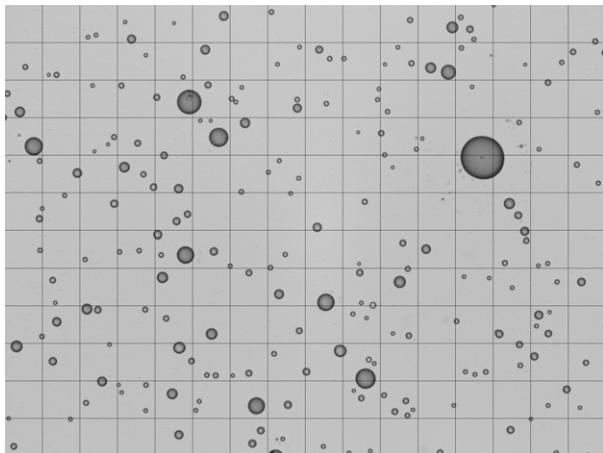
FIG. 2. Image of impacted giant sea-salt aerosol particles on a polycarbonate slide. The slide was exposed on the NSF/NCAR C-130 during the VOCALS deployment on 18 Oct 2008. Prior to being digitally photographed, the slide was inserted into a chamber with a constant relative humidity of 90% for more than 12 h; thus, sea-salt particles become solution cap drops on the slide. The slide is photographed from above, and the grid lines are separated by 37 μm. The largest particle on this image has a calculated equivalent NaCl dry radius $r_d = 6.6\,\mu$m. See also Table 3 and Fig. 1.

off the coast of northern Chile. After exposure, the slides were stored in desiccated test tubes and subsequently analyzed in a microscope laboratory at NCAR. In the laboratory, the slides were inserted into humidified air (RH = 90%) and photographed digitally. One image out of 340 such images from a single microscope slide is shown in Fig. 2; this image was then used to derive the NaCl equivalent particle mass for each imaged GCCN particle using the Kohler equation. The observed GCCN size distribution for all 340 images from the slide contains particles from 0.7- to 9.1-μm dry radius and is shown in Fig. 1 and in table form in Table 3. Tang et al. (1997) have shown that the hygroscopic behavior of NaCl particles is nearly identical to that of pure sea-salt aerosols. At 65% RH, GCCN with $r_d = 5\,\mu$m ($r = 7.5\,\mu$m) have terminal velocities of about $0.01\,\mathrm{m\,s^{-1}}$, thus settling out of a 600-m-deep mixed layer in less than 18 h. Such particles are thus expected to be generated in the VOCALS domain, whereas some much smaller GCCN with longer lifetimes may have been advected in from upwind areas.

The result of the simple adiabatic parcel model calculations are presented in the next section using these aerosol distributions as the cloud condensation nuclei upon which cloud drops can grow. A full description of caveats, simplifications, and limiting assumptions will be given in section 7.

3. Results: Adiabatic condensational drop growth

a. Marine stratocumulus clouds

1) MODIFIED POLLUTED AEROSOL DISTRIBUTION

The result of the first model calculation is shown in Fig. 3, using only submicrometer dry aerosol particles from the modified polluted aerosol distribution. The model is initialized at nearly 300 m below cloud base, where solution drops are in equilibrium with the ambient humidity at 85.6%. Mordy (1959) initialized drops either at equilibrium size at RH = 99% or higher, Cooper et al. (1997) initialized drops at RH = 95% equilibrium size, but the present calculation gives a more accurate description of the changing drop size as they are embedded in a rising airstream. Figure 3 shows 1) ascent from 300 m below cloud base to 300 m above cloud base (to cloud top), with a typical stratocumulus constant updraft of $0.4\,\mathrm{m\,s^{-1}}$ and 2) followed by a descent of 300 m from cloud top to cloud base, in this case with a constant downdraft of $-0.4\,\mathrm{m\,s^{-1}}$. Also shown in Fig. 3 is the drop growth of five representative aerosol sizes (out of 100 aerosol sizes) in the updraft (red curves) and the subsequent downdraft (blue curves). The growth curves span the aerosol size range that lead to activated cloud drops; the smallest aerosols are not activated into cloud drops. The familiar narrowing of the drop size distribution with height in the cloud is visible from the values of the cloud drop spectral parameters given in the top half of Table 4 for selected heights above cloud base.

Drops formed on the smallest of the activated aerosol particles are smaller in downdrafts than in updrafts (Fig. 3; see also Lebo et al. 2008), even to the extent that some evaporate completely in downdrafts before reaching the cloud-base altitude (altitude where saturation was first met in the initial updraft). Drop sizes for many larger aerosol sizes are larger in downdrafts than in updrafts (Fig. 3). Thus, differences in aerosol mass, even for small accumulation-mode aerosol particles, result in different behavior dependent on drop size in up- and downdrafts (see also section 4). The right side of Fig. 3 shows the familiar development of the supersaturation with a peak at the cloud drop activation region in the updraft (red curve) and with a rapid change to a slight negative supersaturation once the downdraft is imposed on the parcel at cloud top (blue curve).

2) MODIFIED POLLUTED + GCCN AEROSOL DISTRIBUTION

Next we add GCCN to the modified polluted aerosol distribution, and the same model is used to calculate

TABLE 3. The GCCN size distribution observed over the southeast Pacific from 1346:37 to 1347:04 UTC 18 Oct 2008, using the GNI external impaction sampler on the NSF/NCAR C-130. The polycarbonate slide was exposed 300 km southwest of Arica, northern Chile, at an altitude of 140 m above the sea surface at a horizontal wind speed of $5.4 \ \mathrm{m\,s^{-1}}$. Sizes and concentrations were determined in a laboratory microscope system using humidified air. The sizes are NaCl equivalent particle sizes, and the total sea-salt loading is $7.3 \ \mu\mathrm{g\,m^{-3}}$. Aerosol spectra are given for bins with 0.2-μm radius width, centered on the r_d values given below. The table shows the observed concentrations in a bin N_a and cumulative concentrations N_{ca} summed over the bin and all larger bins. In all, 340 images, such as the one shown in Fig. 2, were used to obtain the size distribution, and the total sample volume of the analyzed part of the slide was $0.26 \ \mathrm{m^3}$.

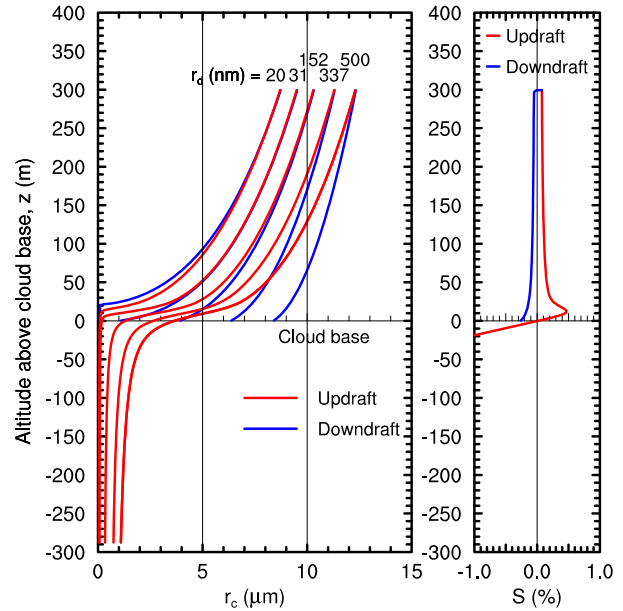| r_d (μm)	N_a (m⁻³)	N_{ca} (m⁻³)	r_d (μm)	N_a (m⁻³)	N_{ca} (m⁻³)	r_d (μm)	N_a (m⁻³)	N_{ca} (m⁻³)	r_d (μm)	N_a (m⁻³)	N_{ca} (m⁻³)	r_d (μm)	N_a (m⁻³)	N_{ca} (m⁻³)
			2.0	5486	19 430	4.0	265.3	1274	6.0	12.95	148.5	8.0	0	9.064
			2.2	3805	13 940	4.2	212.4	1009	6.2	43.23	135.5	8.2	0	9.064
			2.4	2593	10 140	4.4	137.8	796.6	6.4	26.26	92.28	8.4	0	9.064
			2.6	1919	7544	4.6	121.4	658.8	6.6	30.50	66.02	8.6	4.522	9.064
0.8	111 800	281 700	2.8	1278	5626	4.8	100.9	537.4	6.8	4.385	35.52	8.8	0	4.542
1.0	68 490	169 900	3.0	998.4	4347	5.0	122.2	436.5	7.0	4.372	31.13	9.0	4.542	4.542
1.2	38 400	101 400	3.2	777.9	3349	5.2	50.64	314.3	7.2	4.465	26.76			
1.4	21 820	63 040	3.4	519.5	2571	5.4	38.30	263.7	7.4	4.395	22.30			
1.6	13 300	41 220	3.6	400.5	2052	5.6	55.47	225.4	7.6	4.427	17.90			
1.8	8496	27 920	3.8	376.9	1651	5.8	21.45	169.9	7.8	4.411	13.48			

FIG. 3. (left) Condensational drop size as a function of altitude above cloud base for a range of dry NaCl aerosol sizes (labeled at the top of each curve), with concentrations given by the modified polluted case in Table 1. Red curves pertain to an adiabatic updraft of $0.4 \ \mathrm{m\,s^{-1}}$ to cloud top 300 m above cloud base, and blue curves pertain to an adiabatic downdraft of $-0.4 \ \mathrm{m\,s^{-1}}$ from cloud top to cloud base. Cloud liquid water content is $0.58 \ \mathrm{g\,kg^{-1}}$ at cloud top. (right) The supersaturation during the same updraft and downdraft.

drop growth analogous to the previous small CCN-only case. This combined aerosol spectrum resulted in activation of a cloud drop concentration of about $155 \ \mathrm{cm^{-3}}$, which is close to the average cloud drop concentration observed with the cloud droplet probe [CDP; manufactured by Droplet Measurement Technologies (DMT), Boulder, Colorado] for the 80 NSF/NCAR C-130 VOCALS cloud soundings from research flights RF01, RF02, and RF05–RF14 (the flights with good CDP data). In the present case of both modified polluted CCN and added GCCN (Fig. 4), only one submicrometer growth curve is shown ($r_d = 0.1 \ \mu$m), along with nine curves spanning the size range of the observed GCCN particles. Drops formed on GCCN are large, even several hundred meters below cloud base, and they grow strongly as they rise toward cloud base because of their hygroscopic properties.

Within cloud, this drop size distribution (formed on both submicrometer aerosols and GCCN) narrows with altitude (Table 4, bottom half labeled Mod. polluted + GCCN), although it remains wider than the drop size distribution formed only on submicrometer aerosol particles. Overall, the average drop size and width of the drop spectra in Table 3 are little affected by the inclusion

TABLE 4. Drop spectral properties as a function of altitude above cloud base z. The table lists mean cloud drop radius $\bar{r}$, drop spectral width σ, and drop dispersion $\sigma/\bar{r}$. The top part of the table refers to calculations with only submicrometer aerosols from the modified polluted distribution (Mod. polluted; $r_d < 0.5\,\mu m$), and the bottom part refers to calculations with both the modified polluted submicrometer aerosol distribution and giant sea-salt aerosol particles (Mod. polluted + GCCN; $r_d < 9.2\,\mu m$) (see Tables 1 and 3).

Aerosols	z (m)	Updraft			Downdraft		
		$\bar{r}$ (μm)	σ (μm)	$\sigma/\bar{r}$	$\bar{r}$ (μm)	σ (μm)	$\sigma/\bar{r}$
Mod. polluted	300	9.77	0.31	0.032	9.77	0.31	0.032
Mod. polluted	250	9.20	0.32	0.035	9.23	0.33	0.036
Mod. polluted	200	8.54	0.34	0.039	8.57	0.36	0.042
Mod. polluted	150	7.75	0.36	0.046	7.80	0.39	0.051
Mod. polluted	100	6.75	0.38	0.057	6.82	0.45	0.066
Mod. polluted	50	5.28	0.44	0.083	5.43	0.57	0.105
Mod. polluted + GCCN	300	9.77	0.40	0.041	9.77	0.40	0.041
Mod. polluted + GCCN	250	9.19	0.41	0.044	9.21	0.43	0.047
Mod. polluted + GCCN	200	8.52	0.41	0.048	8.56	0.46	0.054
Mod. polluted + GCCN	150	7.73	0.43	0.055	7.78	0.51	0.065
Mod. polluted + GCCN	100	6.73	0.45	0.066	6.79	0.57	0.084
Mod. polluted + GCCN	50	5.26	0.45	0.093	5.38	0.69	0.129

of GCCN. However, this is only part of the picture, because the properties of the many small drops mask the changes happening at the tail of the distribution with the large drop sizes. Figure 4 shows that drops formed on GCCN while in cloud grow much faster by condensation than drops formed on submicrometer aerosol particles; submicrometer drops grow by about 10-μm radius from cloud base to cloud top, whereas, for example, drops formed on GCCN with $r_d = 9\,\mu$m grow by 17 μm from cloud base to cloud top. This is an accelerated drop growth, and the difference in growth rates is contrary to the traditionally assumed $1/r$ growth rate. Accelerated growth of larger drops has also been calculated in prior modeling studies of mixed-phase clouds (i.e., Lebo et al. 2008), but the extent of the growth rates on the present GCCN size distribution is larger because of the inclusion of GCCN sizes to 9-μm dry radius.

What is perhaps even more unexpected is that the drops formed on GCCN of $r_d \gtrsim 2\,\mu$m continue to grow by condensation in cloudy subsaturated downdrafts (blue curves in Fig. 4). This is contrary to the evaporation in downdrafts experienced by drops formed on small accumulation-mode aerosol particles (blue curves in Fig. 3) Condensation makes the largest drops shown grow by more than 5 μm in downdrafts, whereas drops formed on submicrometer aerosol particles evaporate, for a size loss of about 9 μm. Although the behavior of condensational drop growth in downdrafts is most apparent for drops formed on the largest dry radius ($r_d = 9\,\mu$m), the effects remain for drops grown on GCCN sizes with $r_d > 2\,\mu$m.

3) PRISTINE + GCCN AEROSOL DISTRIBUTION

Next we consider drop growth in clean atmospheric conditions with low aerosol concentrations,

as often found in the western part of the VOCALS flight domain. To investigate drop growth in clean atmospheric conditions, we used the Grabowski et al. (2011) pristine aerosol size distribution (see Table 1). The additional GCCN portion of the aerosol spectrum was kept unchanged (Table 3) as wave action and giant aerosol production are assumed independent of the degree of air pollution.
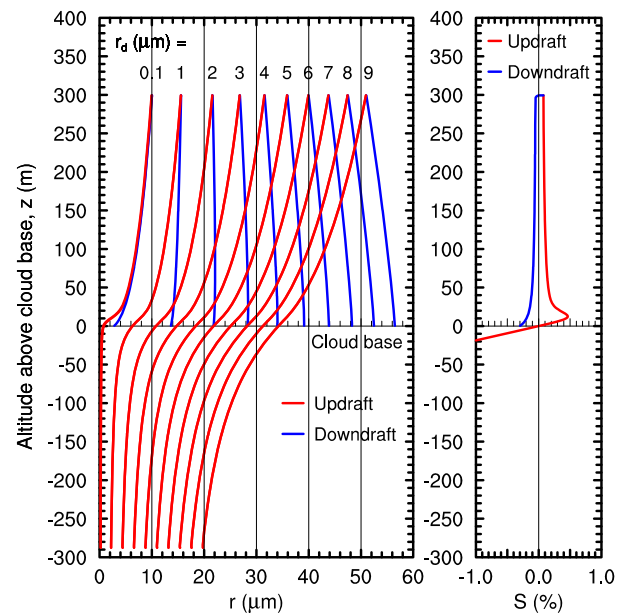

FIG. 4. As in Fig. 3, but for the modified polluted + GCCN case. Note that drops formed on GCCN particles grow considerably in cloud because of condensation, so much so that they accelerate away from the main cloud drop peak (exemplified by $r_d = 0.1\,\mu$m) during upward motion, and that many such drops continue to grow considerably by condensation in the subsaturated downdraft.
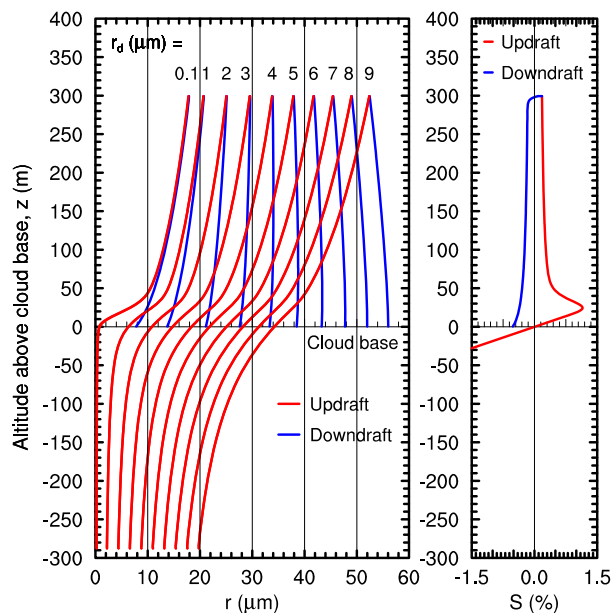
FIG. 5. As in Figs. 3 and 4, but for the pristine + GCCN case. Note that drops formed on small aerosol particles ($r_d \approx 0.1 \, \mu$m) are much larger ($\approx 17 \, \mu$m) at cloud top, in comparison to the modified polluted + GCCN case in Fig. 4. In contrast, drops formed on the largest of the giant aerosols are fairly similar in size to those for more polluted air (Fig. 4). Drops formed on smaller GCCN may grow somewhat faster in this less polluted aerosol environment.

Figure 5 shows the resulting growth curves for a single representative submicrometer aerosol and 9 GCCN size classes, as well as the supersaturation profiles for up- and downdrafts. This clean case has a higher overall supersaturation than the modified polluted case. This is accompanied by a lower drop concentration of about $29 \, \text{cm}^{-3}$ (vs. about $148 \, \text{cm}^{-3}$) at cloud top, and it results in the $r_d = 0.1 \, \mu$m cloud drop growing to $16.7 \, \mu$m (vs. about $9.8 \, \mu$m in the modified polluted case). Note that the largest GCCN particles lead to nearly unchanged condensational drop sizes (cf. Fig. 5 to Fig. 4).

b. Marine cumulus clouds

Based on the pattern of drop growth on GCCN in marine stratocumulus and the saturation ratio relationships [section 3a(2) and later in section 4], it is simple to predict the effects of GCCN condensational drop growth in small adiabatic marine cumulus. Such small cumulus include trade wind cumulus (Rauber et al. 2007), cumulus rising into an overlying marine stratus deck (Jensen et al. 2000), and the similar cumulus rising into overlying stratus in the western part of the VOCALS domain (Cui et al. 2014, their Fig. 15). Based on sections 2a and 3a(2) and later in section 4, it can be expected that, for a given GCCN size distribution, residence time in cloud is likely a critically important factor
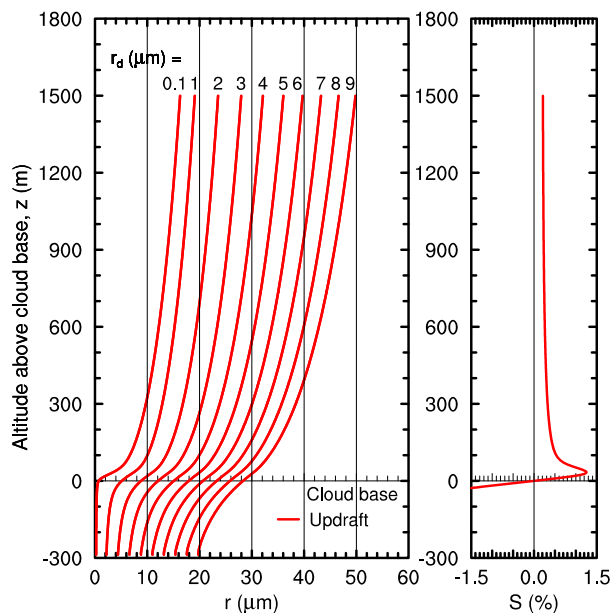
FIG. 6. Drop growth curves for a simulated cumulus cloud. As in Fig. 4 with modified polluted + GCCN, but for an updraft of $2 \, \text{m s}^{-1}$ and for a 1500-m-deep cloud. Only updraft curves are shown.

to determine the condensational growth of the largest GCCN since GCCN drops often grow throughout their entire time in cloud, regardless of vertical motion.

To test this, a calculation was done with a steady updraft of $2 \, \text{m s}^{-1}$ (typical of many small marine cumulus) and for a total cloud height of 1500 m, both values 5 times greater than the marine stratocumulus case presented in section 3a(2). The calculation, using the modified polluted size distribution (Table 1) and the GCCN size distribution (Table 3) resulted in activation of a drop concentration of $\approx 157 \, \text{cm}^{-3}$. Figure 6 shows that drop growth on GCCN at 1500 m above cloud base is similar to those at the top of the marine stratocumulus (Fig. 4), in particular for those grown on the largest of the GCCN. We note that the time in cloud for ascent to cloud top is 750 s for both cases and that the drop growth for the largest GCCN is remarkably similar for the stratocumulus and cumulus cases, further emphasizing the importance of time spent in cloud.

4. Supersaturation and accelerated drop growth of GCCN drops

To understand the growth rates for drops formed on large GCCN, it is necessary to examine the difference between the actual saturation over pure water and the effective saturation for a solution drop. In examining drop growth, it is often convenient to discuss the
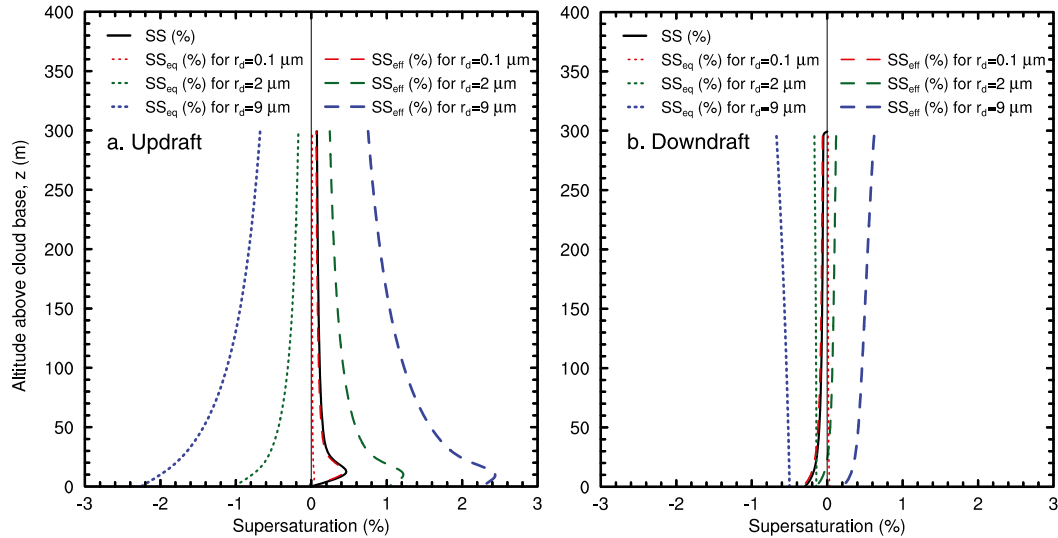
FIG. 7. Altitude variation of actual supersaturation SS (solid), equilibrium supersaturation SS_{eq} (dotted), and effective supersaturation SS_{eff} (dashed) in (a) an updraft of $0.4 \, m \, s^{-1}$ and (b) a downdraft of $-0.4 \, m \, s^{-1}$ for aerosol particles of $r_d = 0.1 \, \mu m$ (red), $r_d = 2 \, \mu m$ (green), and $r_d = 9 \, \mu m$ (blue). This case uses the modified polluted + GCCN aerosol spectrum.

supersaturation SS (%) instead of saturation ratio S. The supersaturation is defined as

$$SS = 100 \times (S - 1). \qquad (8)$$

Figure 7a compares the actual supersaturation SS, the equilibrium supersaturation SS_{eq}, and the effective supersaturation SS_{eff} for three different aerosol sizes: $r_d = 0.1$, 2, and 9 μm. Here, the equilibrium supersaturation SS_{eq} (%) is defined as

$$SS_{eq} = 100 \times (S_{eq} - 1). \qquad (9)$$

For a given GCCN mass m_s and drop size r, a GCCN drop may be in equilibrium ($dr/dt = 0$) at a relative humidity of, for example, 99% because of the large salt content, or equivalently, a value of SS_{eq} of -1%.

The difference between the actual supersaturation and the equilibrium supersaturation is thus the effective supersaturation SS_{eff}:

$$SS_{eff} = SS - SS_{eq}. \qquad (10)$$

For a typical cloudy supersaturation of 0.2% in an updraft, and for the example of an equilibrium supersaturation of -1% for a drop formed on a GCCN, the effective supersaturation in this case results in $SS_{eff} = 1.2\%$. Thus, for GCCN drops, it is possible to have the effective supersaturation be many times more than the actual supersaturation (in this hypothetical case 6 times more). In comparison to normal cloud drops

formed on small aerosol particles, this higher effective supersaturation is the key reason that GCCN drops grow faster by condensation in clouds; see also Kulmala et al. (1997).

Returning to the parcel model calculation for calculating updraft conditions, the actual supersaturation is the familiar black curve in Fig. 7a. The equilibrium supersaturation for small aerosol particles is slightly positive (red dotted curve), which is typical for dilute drops, but the equilibrium supersaturation of drops formed on the two GCCN sizes is still much less than zero (concentrated solution drops; green and blue dotted curves) while in cloud in the updraft. However, the effective supersaturation [Eq. (10)] is very large for both displayed GCCN sized particles (green and blue dashed curves). At cloud top in this imposed updraft, the effective supersaturation for a drop formed on a GCCN of $r_d = 9 \, \mu m$ is 11.5 times larger than the actual supersaturation at that level. This clearly indicates that drops formed on large GCCN cannot be considered dilute drops and that they primarily grow condensationally by being hygroscopic, not by the relatively small actual supersaturation in cloudy updrafts. Importantly, the growth rates of drops formed on the largest GCCN are nearly identical in both the polluted environment (Fig. 4) and the pristine environment (Fig. 5) because in both cases their effective supersaturations SS_{eff} are much larger than the actual supersaturation SS.

In downdrafts, the actual supersaturation SS is negative (Fig. 7b, black curve), and the effective
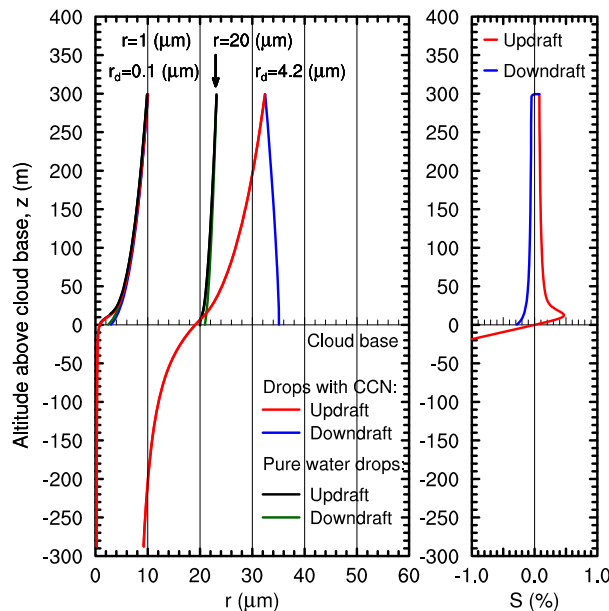
FIG. 8. Condensational drop growth curves for a comparison of pure water drops and drops on GCCN. Red and blue curves have the same conditions as in Fig. 4, but black and green curves are for pure water drops. The growth curve for a pure water drop initiated at $r = 1\,\mu m$ virtually coincides with the curve for drops grown on $r_d = 0.1$-μm aerosol particles. At cloud base, the large pure water drop initiated as $r = 20\,\mu m$ has the same size as the drop grown on an $r_d = 4.2$-μm GCCN; however, the drops grown on GCCN grow much more rapidly than the pure water drops.

supersaturation SS_{eff} for GCCN drops is somewhat reduced though still positive (green and blue dashed curves), yet drops formed on the largest GCCN still grow considerably by condensation in the downdraft because they are concentrated solutions; this is in contrast to normal dilute cloud drops (formed on small aerosol particles; red dotted and dashed curves) that evaporate in cloudy downdrafts because of their negative SS_{eff}.

5. The pure water hypothesis after drop activation

a. Drop growth through condensation

Several microphysics studies have attempted to represent the GCCN effect by adding large water drops to the drop spectrum at cloud base. For instance, in order to simulate the effect of GCCN drops Feingold et al. (1999) added drops of $r = 20\,\mu m$ at cloud base of a marine stratocumulus but subsequently used the droplet growth equation without the solute term. In the marine cumulus study of Kogan et al. (2012), drops of up to $r = 31.5\,\mu m$ were added at cloud base in place of tracking GCCN mass in the cloud drops. Likewise, for a

climate model simulation of the effects of GCCN, Posselt and Lohmann (2008) added pure water drops of $r = 20\,\mu m$ instead of tracking aerosol mass in GCCN drops. This goes some way toward representing GCCN, but it omits the added condensational effect of the solute material in drops formed on GCCN while in cloud.

Figure 8 shows the drop growth curves for a subset of the accumulation-mode and GCCN sizes previously displayed, with the addition of curves for pure water drops with radii of 1 and $20\,\mu m$ at cloud base. The growth curves for pure water drops with $r = 1\,\mu m$ at cloud base, similar to the Khairoutdinov and Kogan (2000) bin-microphysics large-eddy simulation study, are virtually similar to the growth curves for drops formed on an accumulation-mode aerosol particle of $r_d = 0.1\,\mu m$. Such drops formed on accumulation-mode aerosol particles can thus be considered dilute a short distance above cloud base.

In Fig. 8, the larger pure water drop only grows from $r = 20\,\mu m$ to $r = 23.2\,\mu m$ from cloud base to cloud top. For the same updraft, a GCCN particle with $r_d = 4.2\,\mu m$ likewise has a radius of about $20\,\mu m$ at cloud base but grows much more to $r = 32.4\,\mu m$ at cloud top and then even more in the subsequent downdraft to $r = 35.1\,\mu m$. Retaining the solute term in the drop growth equation versus assuming pure $r = 20$-μm water drops results in about 4 times larger condensational growth from cloud base to cloud top. One way of viewing this is to recognize that growth of the pure water drop largely follows the $(S - 1)/r$ relationship from the drop growth equation, whereas the drops with large GCCN solute mass mainly grow condensationally in response to SS_{eff}, dominated by the solute term of the drop growth equation, as opposed to the actual supersaturation SS.

b. Drop growth through condensation and coalescence

It is clear that GCCN mass has a major impact on condensational drop growth, even past the traditional threshold for drizzle drops, for example, $r = 20\,\mu m$ (Wood 2005) or $r = 25\,\mu m$ (Khairoutdinov and Kogan 2000), but is this condensational growth important in comparison to the coalescence growth of such drops?

To answer this question, we add a gravitational coalescence calculation [see Eqs. (B16)–(B18) in appendix B] to the results shown in Fig. 8; that is, we compare the total drop growth (condensation and coalescence) for the pure water drop initiated with $r = 20\,\mu m$ at cloud base to the similar total drop growth (condensation and coalescence) for the drop formed on a GCCN particle with $r_d = 4.2\,\mu m$, which likewise has $r \approx 20\,\mu m$ at cloud base. The results are shown in Fig. 9. Only a subset of the
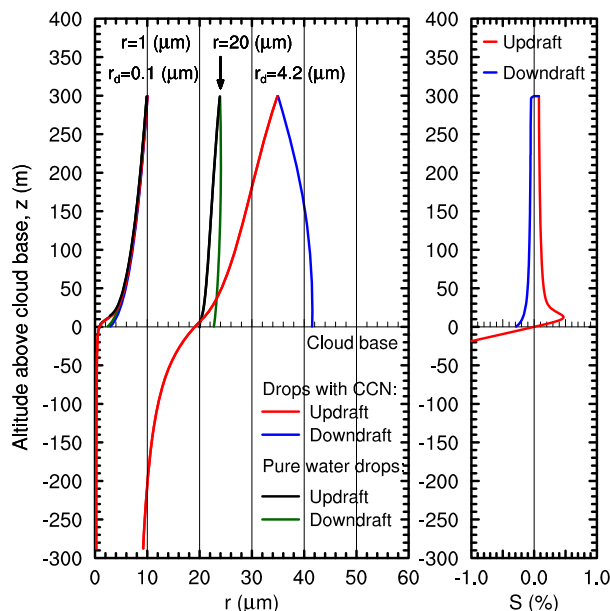
FIG. 9. As in Fig. 8, but with inclusion of both condensation and gravitational coalescence (see text in section 5b). Both the pure water drop initiated at $r = 20\,\mu m$ and the GCCN drop with the same size at cloud base grow by condensation and gravitational coalescence as a result of collection of smaller drops (e.g., drops grown on $r_d = 0.1$-μm aerosol particles, curve included for reference). But the added effect of coalescence growth is much stronger for the GCCN drop than for the pure water drop (cf. to Fig. 8).

drop sizes are shown: 1) drops grown on accumulation-mode aerosols (curves for $r_d = 0.1\,\mu m$ red and blue), 2) the growth curves of a pure water drop initiated with $r = 20\,\mu m$ at cloud base (black and green curves), and 3) the growth curves of a GCCN drop formed on an $r_d = 4.2$-μm particle (red and blue curves).

The case demonstrated in Figs. 8 and 9 pertains to a cloud drop distribution with a mean radius of $9.8\,\mu m$ at cloud top; that is, so small that the cloud is not normally assumed to have vigorous warm rain formation (e.g., Rosenfeld and Lensky 1998). Yet the growth curves for the two cases of large drops (pure water and GCCN, respectively) in Fig. 9 demonstrate that the condensational effect of large GCCN persists far into the size range normally associated with drizzle drop sizes and coalescence: as previously shown in Fig. 8, the pure water drop, initiated with $r = 20\,\mu m$ at cloud base grows to $r = 22.2\,\mu m$ at cloud top ($r = 20.9\,\mu m$ at cloud base on return) when only condensation is included, and it grows to $r = 23.9\,\mu m$ at cloud top ($r = 22.7\,\mu m$ at cloud base) when both condensation and coalescence are included (Fig. 9).

In contrast, the GCCN drop formed on an $r_d = 4.2\,\mu m$ ($\approx r = 20\,\mu m$ at cloud base) grows to $r = 32.4\,\mu m$ at cloud top ($r = 35.1\,\mu m$ at cloud base on return) when

only condensation is included (Fig. 8), and it grows to $r = 34.9\,\mu m$ at cloud top ($r = 41.5\,\mu m$ at cloud base) when both condensation and coalescence are included (Fig. 9). Thus, the drop formed on $r_d = 4.2\,\mu m$ reaches close to double the size of the pure water drop when both condensation and coalescence are accounted for.

This demonstrates that retaining the solute term for condensational growth of drops formed on GCCN, even in the presence of coalescence, for this case leads to growth rates that are also 4 times larger than that of drops initiated as pure water drizzle-sized drops at cloud base. Thus, condensational growth of drops formed on GCCN particles is important for the subsequent growth of drizzle-sized drops, and inserting pure water drops of $r = 20\,\mu m$ at cloud base as done in, for example, Feingold et al. (1999) and Posselt and Lohmann (2008) may have underestimated the effect of GCCN on warm rain formation.

We have done the same calculations for pristine air with GCCN particles and for 1) condensation only and 2) condensation and coalescence. The result (not shown) is that the condensational growth of drops formed on GCCN leads to growth rates that are about 2 times larger than that of drops initiated as pure water drops at cloud base. Thus, even in pristine air, condensational growth of drops formed on GCCN particles is important for the subsequent coalescence growth of drizzle-sized drops.

6. GCCN sizes and rainfall flux

The observed VOCALS GCCN spectrum (Table 3) covers dry radii from 0.8 to $9\,\mu m$, but what part of this size range is responsible for most of the rainfall rate? Is it the numerous small GCCN, the few very large GCCN, or the intermediate range with total particle concentration of a few to tens per liter? In the VOCALS observations, and in shallow clouds in general, rain rates are usually small. It is in these lightly raining or marginal scenarios that we expect GCCN to have the largest impact.

The parcel model is run as previously, but in this case for cloud depths of 300, 400, and 500 m, for an updraft of $0.4\,m\,s^{-1}$. Adiabatic liquid water contents at cloud top for these three cases are 0.58, 0.75, and $0.93\,g\,m^{-3}$, respectively. Aerosols are specified in two ways: 1) as modified polluted in combination with GCCN, and 2) as pristine in combination with GCCN. Thus, for a total of six model runs, we calculate the precipitation flux at cloud base on descent for all accumulation-mode particles (summed to a single flux) and also independently for each of the 44 sizes of GCCN particles. The results are shown in Fig. 10; note that the curves are not smooth
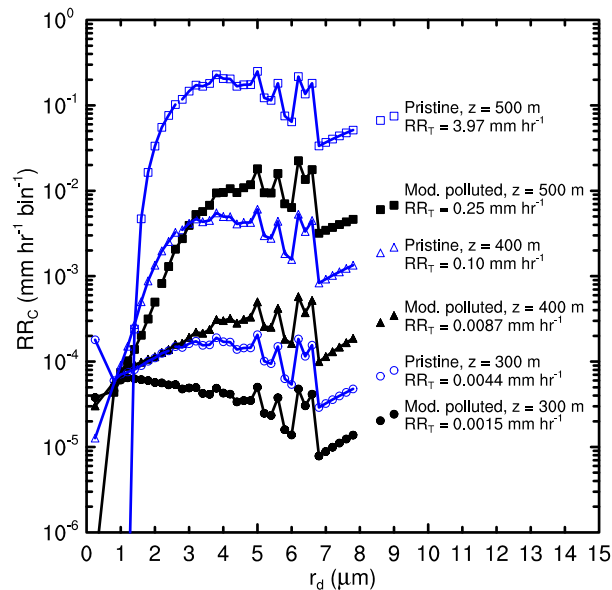
FIG. 10. Contribution to rain rate RR_C for drops grown on GCCN particles as a function of dry aerosol size for the cases of small aerosol particles given by the modified polluted and pristine size distributions. The contribution of all accumulation-mode particles is summed up and shown with the symbols at dry radius $r_d = 0.25\,\mu m$. All other symbols refer to the GCCN particles listed in Table 4. The figure also lists cloud depth z and total rain rate RR_T.

because the GCCN distribution (see Fig. 1) is not smooth for the largest GCCN radii. Three cases have insignificant rain rate (here taken as total rain rate $RR_T < 0.1\,\mathrm{mm\,h^{-1}}$), including the two 300-m cases and the modified polluted 400-m case. For the three cases with significant total rain rate (total rain rate $RR_T = 0.1$–$4\,\mathrm{mm\,h^{-1}}$), the only important contribution to rain rate occurs for drops initially formed on GCCN particles. For these, the contribution to rain rate is strongest for drops formed on GCCN with $r_d > 2\,\mu m$, and in particular for GCCN sizes in the 3–7-μm range, because of a combination of GCCN sizes and concentrations (see Fig. 10). We find that when there is significant rain rate ($RR_T > 0.1\,\mathrm{mm\,h^{-1}}$), the relative contribution from drops initially formed on submicrometer aerosol

particles is negligible. Thus, GCCN completely dominate significant rainfall formation in these clouds, as a result of their strong condensational growth. For example, in the 500-m case, GCCN with $r_d > 2\,\mu m$ account for 98.6% of the total rainfall flux (Table 5). Thus, the impact of GCCN on rainfall increases with increasing cloud depth. These results generally agree with the conclusions of Segal et al. (2004), who found that in a model of precipitation formation, the largest growth occurred from hygroscopic flare seeding when the mass of the seeding material was used to form aerosols with dry radius of 2–3 μm.

7. Discussion

At present time, with current computational resources, cloud modeling studies are generally done one of two ways: 1) they include a fairly complete representation of cloud dynamical aspects but use simple methods for representing cloud microphysics, or 2) they use simple methods for representing cloud dynamics but use a more full representation for cloud microphysics. In this study, we apply the second type but still feel there are important implications shown by our study despite the limitations posed by the assumed simple dynamics and lack of sedimentation.

This study has focused on the impact of condensational growth of drops formed on giant sea-salt aerosol particles in idealized marine stratocumulus and cumulus environments. We have used an adiabatic parcel model, with simple kinematic motion ($0.4\,\mathrm{m\,s^{-1}}$ updraft to cloud top, followed by $0.4\,\mathrm{m\,s^{-1}}$ downdraft to cloud base) and with a fairly complete condensation description, including treatment of drops as solution drops both below and above cloud base. Given that the largest drops grow to $r = 55\,\mu m$ for a 300-m cloud depth, it is clear that the neglect of sedimentation of drops imposes limits on the absolute accuracy of the results. The terminal velocities of drops with radii of 20, 35, and $50\,\mu m$ are about 0.05, 0.13, and $0.26\,\mathrm{m\,s^{-1}}$, respectively. These are small, but not insignificant in comparison to the assumed $0.4\,\mathrm{m\,s^{-1}}$ updraft speed. A sedimenting

TABLE 5. Total rain rate RR_T (mm h^{-1}), and contribution to total rain rate RR_C (mm h^{-1}) and RR_C/RR_T (%), of drops grown on GCCN larger than threshold sizes and ranges for r_d. Cases with rain rate in excess of 0.1 mm h^{-1} are shown in bold.

Aerosols	z (m)	RR_T (mm h^{-1})	$2\,\mu m < r_d$		$3 < r_d < 7\,\mu m$	
			RR_C (mm h^{-1})	RR_C/RR_T (%)	RR_C (mm h^{-1})	RR_C/RR_T (%)
Mod. polluted + GCCN	300	0.001 47	0.001 02	69.4	0.000 67	45.6
Mod. polluted + GCCN	400	0.008 69	0.006 65	76.5	0.005 98	68.9
Mod. polluted + GCCN	500	**0.2477**	**0.2463**	**99.4**	**0.206**	**83.2**
Pristine + GCCN	300	0.004 43	0.003 66	82.7	0.002 63	59.4
Pristine + GCCN	400	**0.104**	**0.100**	**96.8**	**0.0760**	**73.4**
Pristine + GCCN	500	**3.97**	**3.91**	**98.6**	**3.09**	**77.9**

drop will, in general, have a longer residence time in a sustained updraft and a shorter residence time in a sustained downdraft, with a net shorter time in cloud. Considering the importance of time in cloud for condensational growth, the neglect of sedimentation is a noteworthy exception that should be considered in future improvements to the study of droplet growth. An additional aspect relevant for residence time includes the liquid water content, which affects the rate of coalescence growth and thus a droplet's fall velocity. For the calculations with drop coalescence, we have used a simple gravitational coalescence scheme [Eqs. (B16)–(B18)]. The omission of turbulent enhancement to collision efficiencies is largely justified because of the typically low turbulent energy dissipation rates in marine stratocumulus (e.g., average values of less than $10^{-3}\,\mathrm{m}^2\,\mathrm{s}^{-3}$) (Lothon et al. 2005).

It is well established that GCCN are ubiquitous in marine boundary layer cloud environments (see review in Lewis and Schwartz 2004), and it is well established that such GCCN attain sizes of up to 10-μm dry radius (e.g., Woodcock 1953, his Fig. 1, Beaufort wind force 3–5; see also Jensen and Lee 2008, their Fig. 1). When considering condensational growth, GCCN have two distinct advantages over submicrometer-sized accumulation-mode aerosol particles: 1) they form large drops even before entering cloud base, and 2) they may remain highly concentrated solution drops for long durations in cloud, resulting in an effective supersaturation that may be many times larger than the actual supersaturation (Fig. 7a). In our case, condensational growth continues for GCCN with $r_d > 2\,\mu$m even in subsaturated downdrafts, where normal cloud drops evaporate toward smaller sizes (Fig. 4).

The second GCCN advantage (high effective supersaturation experienced by GCCN drops) alone results in a condensational growth rate of drops on GCCN that is many times larger than that of similarly sized pure water drops at cloud base (e.g., a factor of 4 apparent from Fig. 8). Drops formed on GCCN accelerate away from the main drop peak, and, while they are relatively few in number, they become larger than others, thereby creating a tail of very large drops. For drops growing on GCCN, the amount of time spent in cloud is much more important than the actual value of supersaturation because of the dominance of the solute term in the drop growth equation [Eq. (1)]. It is because of this solute term domination that many drops formed on GCCN continue to grow by condensation throughout the duration of their time in cloud, almost regardless of actual saturation and direction of vertical motion. Given that the airflow into and out of marine clouds only has a limited time available for warm rain formation,

condensational growth on GCCN is important to consider, as it is a mechanism that contributes to rapid growth of cloud drops up to drizzle and precipitation sizes (e.g., Figs. 4, 5, 6). For these reasons, when modeling shallow convective marine clouds, it is important to include a complete aerosol spectrum that stretches from the small aerosol particles (those that do not activate in updrafts), through submicrometer accumulation-mode particles (that form the majority of cloud drops), all the way up to and including GCCN (which make the largest drops).

Aerosols and the cloud droplet spectrum are not the only factors to consider when understanding this simple model study of droplet growth. Other factors include the following: 1) Our modeling was restricted to shallow marine clouds with relatively low liquid water contents that are only expected to produce marginal amounts of rain or drizzle. 2) It is in these marginal cases that prior studies have shown GCCN make the largest difference (e.g., Feingold et al. 1999). 3) Our neglect of sedimentation and our prescribed updraft and downdraft velocities have strong control over time in cloud, a critical variable in condensational growth, which ultimately limits the conclusions that can be drawn from this study.

Some bin-microphysics models treat a one-dimensional aerosol spectrum, covering most of the range of sea-salt GCCN. For instance, Kogan (1991) describes a model with the ability to have 19 size bins of aerosol particles with dry radii from 0.0076 to 7.6 μm. However, Kogan (1991) only considers the solute term during the activation process [through a parameterization based on Ivanova et al. (1977)], after which the solute term is omitted (see Kogan 1991, p. 1164). The present study demonstrates that the solute term for drops in the GCCN size range remains important relative to the ambient supersaturation, in some cases for tens of minutes after air enters the cloud.

A number of other studies likewise have the ability to treat aerosols over the entire size range, including GCCN. For instance, in a marine stratocumulus modeling study, Khairoutdinov and Kogan (1999) used measurements from a Passive Cavity Aerosol Spectrometer Probe (PCASP) (see Martin et al. 1994) with a radius range of 0.05–1.5 μm. Thus, larger aerosols could be generated through drop coalescence, but they were apparently not part of the initial aerosol spectrum. In more recent studies, Andrejczuk et al. (2008) used an aerosol range with maximum size of $r_d = 1\,\mu$m, and Andrejczuk et al. (2010) used a maximum $r_d = 3\,\mu$m. In the bin-microphysics calculation of Grabowski et al. (2011), a maximum radius of 0.25 μm was assumed. Thus many bin-microphysics schemes assume smaller initial GCCN particles than observed below the VOCALS marine stratocumulus (Fig. 1).

In the study of Feingold et al. (1996), a single log-normal distribution was used for 14 bins with a range of 0.0056–7.6 μm, but the lognormal distribution was too narrow in comparison with observed marine GCCN spectra. Thus, the cumulative concentration of particles with $r_d > 2\,\mu$m is about a factor of 1000 larger for the GNI observed GCCN spectrum (Table 3) than it is for the Feingold et al. (1996) lognormal distribution. Likewise, using an improved scheme tracking both aerosol mass and aerosol number, Feingold et al. (1999) included aerosols in the size range of 0.015–7.3 μm and only used a slightly wider lognormal distribution; however, they added 1 and 10 L^{-1} of GCCN with $r_d > 5\,\mu$m but omitted the solute term in the droplet growth equation (W. Cotton 2016, personal communication).

Some bin-microphysics studies track a size distribution of solute mass for each drop size bin [e.g., Bott (2001) through coalescence, and Lebo and Seinfeld (2011) for both coalescence and condensation], but this implies usage of $I_1 \times I_2$ bins to account for I_1 drop classes and I_2 solute mass classes. In comparison, some earlier bin-microphysics models tracked I_1 drop size bins and I_2 solute mass bins (for a total of $I_1 + I_2$ bins). The use of $I_1 \times I_2$ bins vastly increases the memory requirement and computational time. Despite the additional computational cost, the results presented in this study using our simple model demonstrate that it is important to treat the rapid condensational growth of drops formed on GCCN particles in cloud, as these may have condensational drop growth rates that are up to 12 times faster than dilute drops (Fig. 7a). Furthermore, it is likely that studies that add large pure water drops as a substitute for GCCN (e.g., Posselt and Lohmann 2008) have underestimated, potentially by a large amount, the precipitation-forming effect of GCCN particles by assuming pure water drops above cloud base.

The neglect of GCCN and of the solute term in the drop growth equation of models has broad-reaching impacts. Part of the significance of rapid condensational growth creating large drops comes in their ability to accelerate rain formation. Large drops broaden the drop spectrum and have larger swept areas and higher collision efficiencies. The initial advantage of condensation on GCCN particles can have a ripple effect that propagates throughout the rain formation process. A concrete example of drop spectrum broadening is shown in Fig. 4. Because of its simplicity while including both small and giant aerosols, it could be used as a reference against which other drop broadening mechanisms are evaluated. At present, we know of no other mechanisms that can realistically lead to drops of 34-μm radius at cloud base in rising airstreams, followed by continuing strong condensational growth above.

The additional impacts of coalescence are shown in Figs. 9 and 10 and further reinforce the argument of GCCN particles accelerating precipitation formation. Even when coalescence is included, the condensational growth of GCCN particles remains important. A further look at which sizes of GCCN are most important for rain rate shows that GCCN larger than $r_d > 2\,\mu$m carry most of the rainfall flux. In particular, GCCN particles in the size range of 3–7-μm dry radius are most important. As these results are obtained for a model with drop coalescence, but without sedimentation, we caution about absolute accuracy of the calculated rainfall rates, in particular as some drops attain fall speeds approaching 4 m s^{-1}: that is, much larger than the assumed 0.4 m s^{-1} updraft. However, we believe that the following conclusion from Fig. 10 is robust: drops grown on small aerosols do not contribute much to initializing drizzle, especially in cases with significant drizzle (i.e., in the 400- and 500-m-deep clouds in Fig. 10).

8. Summary

Giant sea-salt aerosols (GCCN) are ubiquitous in the marine boundary layer and high-quality measurements of GCCN have been available for the last six decades as a function of wind speed (Woodcock 1953). For the VOCALS domain that covers one of the largest marine stratocumulus regions, the largest GCCN are locally generated, whereas the smallest may contain a large component of GCCN that are advected in.

With the use of a simple drop growth model (adiabatic parcel, condensation, gravitational coalescence, but no sedimentation and no turbulent enhancement to coalescence) we explore the condensational growth of drops on GCCN for two shallow cloud environments, building off of work done by Mordy (1959). We demonstrate that the sizes of drops grown on GCCN in a polluted stratocumulus environment rapidly accelerate away from the main drop peak; thus, the typical narrowing of the drop spectrum assumed with height is not true for drops formed on GCCN. The same behavior occurs in more pristine stratocumulus environments as well as in moderately polluted cumulus environments.

The actual cloudy supersaturation is not highly important for growth of drops on GCCN in cloud because the growth rate depends mostly on the solute term in the drop growth equation. For this reason, drops on large GCCN grow even in subsaturated downdrafts, and thus the duration of time a GCCN drop spends in cloud is especially important. Stronger conclusions cannot be drawn because of the lack of drop sedimentation in our

model, because of the simple prescribed air motions, and because of the omission of mixing and other dynamical processes.

The pure water hypothesis (neglecting the solute term) was tested, and we show that pure water drops, even large ones, do not grow as rapidly as concentrated solution drops formed on GCCN. We demonstrate that 1) even in the presence of coalescence in a cloud, condensational growth of drops formed on GCCN remains highly important while the GCCN is in a cloud and 2) that for the present observed marine GCCN spectrum, drops formed on GCCN particles with dry radius larger than $2\,\mu\mathrm{m}$ dominate the precipitation flux at cloud base and that GCCN with dry radii of sizes $3–7\,\mu\mathrm{m}$ are especially important. Thus, GCCN are very efficient at converting cloud water to rainwater. Finally, adiabatic parcel models can produce significant warm rain, as also observed in some marine stratocumulus, provided that observed GCCN are included as an integral part of the CCN spectrum.

Many studies, including numerous process and climate models, state that they model marine stratocumulus, yet they do not include the effect of GCCN on warm rain formation. We argue that those cloud studies may simulate clean environments, but in the absence of including GCCN and without retaining the solute term in the drop growth equation, they cannot claim to simulate clean marine environments in their treatment of aerosol–cloud interaction.

When calculating warm rain formation in shallow marine environments, condensational growth on drops formed on GCCN must be included to accurately represent the processes at play. The overall conclusion of this simple process model study is that considering all drops as dilute in marine clouds is a poor approximation. Unfortunately, this assumption has been widely used in past studies.

APPENDIX A

List of Symbols

See symbol list in Table A1.

APPENDIX B

Equations for the Adiabatic Parcel Model

Adiabatic Lagrangian parcel models are well suited to calculate the droplet growth for a population of CCN particles. We here calculate the condensational drop growth on I size classes of different aerosol particles radius, where $I = 100$ different size classes for the runs with only small aerosol particles (CCN), and $I = 142$ size classes for runs with both small CCN and GCCN. The aerosol size classes (subscript i) have particle concentrations N_i, aerosol mass classes m_{si}, dry aerosol radius classes r_{di}, and cloud drop radius classes r_i. For simplicity, all particles are assumed to consist of NaCl and thus neglect the effect of soluble gases (Kulmala et al. 1997). Many previous studies have described equations for such models; in the present case there are differential equations for condensational drop growth of drop radius r_i, water vapor mixing ratio q_v, temperature T, air density r_i, and altitude z. The parcel moves kinematically with constant updraft speed w (typically $0.4\,\mathrm{m\,s^{-1}}$) to cloud top, followed by a constant downdraft speed $(-0.4\,\mathrm{m\,s^{-1}})$ to cloud base. The model is initialized nearly $300\,\mathrm{m}$ below cloud base (see Table 2), where solution drops are assumed to be in equilibrium with the ambient humidity. A complete symbol list is given in appendix A; here, only the most important physical quantities will be called out.

The model does not include sedimentation of drops; this is a simplification that limits the main utility to smaller drops and that introduces added uncertainty for the largest drops with terminal velocities approaching or exceeding the main updraft speed of $0.4\,\mathrm{m\,s^{-1}}$. The contribution of radiation to cloud drop growth (Roach 1976; Lebo et al. 2008) is also excluded, as is turbulent enhancement to gravitational coalescence (Franklin et al. 2005); the focus of the current set of calculations is on the impact of a wide range of aerosol sizes on drop growth. The model uses a moveable grid in radius space, such that drops of a given size class all have the same size and all grow (or evaporate) at the same rate. The condensational growth of droplet radius r_i formed on an aerosol with size index i is

$$\frac{dr_i}{dt} = \frac{G}{r_i}(S - S_{\mathrm{eq}}). \qquad (\mathrm{B1})$$

The change in water vapor mixing ratio q_v is given by

$$\frac{dq_v}{dt} = \sum_{i=1}^{I} 4\pi\rho_w N_i r_i^2 \frac{dr_i}{dt}. \qquad (\mathrm{B2})$$

TABLE A1. Symbol list.

Numerator of the surface and solute term of drop growth equation	a and b
Heat capacity of air at constant pressure	c_p
Actual and saturated vapor pressure	e and e_s
Gravitational acceleration	g
Index for small and large aerosols or drops	i and j
Dry aerosol mass	m_s
Pressure	p
Actual and saturated water vapor mixing ratio	q_v and q_{vs}
Dry aerosol radius and drop radius	r_d and r
Mean radius of a drop size distribution	$\bar{r}$
Numerator of the surface and solute term of drop growth equation	a and b
Time	t
Drop terminal fall velocity	v_t
Vertical air velocity	w
Height	z
Water vapor diffusivity and kinetically corrected water vapor diffusivity	D' and D
Drop collision efficiency	E
Inverse of denominator in drop growth equation	G
Total number of aerosol or drop bins	I or J
Moist static energy	H
Thermal conductivity and kinetically corrected thermal conductivity	K' and K
Latent heat of vaporization	L_v
Molality	$\mathscr{M}$
Molecular weight of dry air, water vapor, and NaCl	M_d, M_w, and M_s
Aerosol concentration or drop concentration in a size class	N
Total aerosol concentration	N_a
Gas constant for dry air and vapor	R_d and R_v
Total rain rate and aerosol size dependent rain-rate contribution	RR_T and RR_C
Ambient saturation ratio and supersaturation of water vapor	S and SS
Effective saturation ratio and supersaturation of water vapor	S_{eff} and $\mathrm{SS}_{\mathrm{eff}}$
Equilibrium saturation ratio and supersaturation of water vapor	S_{eq} and $\mathrm{SS}_{\mathrm{eq}}$
Temperature	T
Valence of NaCl	$\mathscr{V}$
Condensation coefficient and thermal accommodation coefficient	α_c and α_T
Air, water, and NaCl density	ρ_a, ρ_w, and ρ_s
Standard deviation of a drop size distribution	σ
Surface tension of water against air	σ_w
Jump lengths for condensation and heat	Δ_c and Δ_T
Chemical potential of NaCl	Φ_s

Temperature is integrated based on the assumption that the moist static energy $H = c_p T + L_v q_v + gz$ is constant in an adiabatic process so that

$$\frac{dT}{dt} = -\frac{L_v}{c_p}\frac{dq_v}{dt} - \frac{g}{c_p}\frac{dz}{dt}. \tag{B3}$$

The evolution of air density ρ_a, is described by

$$\frac{d\rho_a}{dt} = -\frac{\rho_a g w}{R_d T} - \frac{\rho_a}{T}\frac{dT}{dt}, \tag{B4}$$

which can be derived from the equation of state and the hydrostatic equation. Altitude z is calculated from

$$\frac{dz}{dt} = w. \tag{B5}$$

Pressure is diagnosed from

$$p = \rho_a R_d\left(1 + \frac{M_w}{M_d}q_v\right). \tag{B6}$$

The actual saturation ratio S over pure water is given by

$$S = \frac{q_v}{q_{vs}}. \tag{B7}$$

The saturated vapor mixing ratio is given by

$$q_{vs} = \frac{\dfrac{M_w}{M_d}e_s}{p - e_s}, \tag{B8}$$

where the saturated vapor pressure e_s is from Bolton (1980).

The term containing the denominator of the condensational droplet growth equation G is given by

$$G = \cfrac{1}{\cfrac{\rho_w R_v T}{e_s D} + \cfrac{\rho_w L_v}{KT}\left(\cfrac{L_v}{R_v T} - 1\right)}. \quad \text{(B9)}$$

Water vapor diffusivity D' (m^2 s^{-1}; excluding kinetic effects) is given by Grabowski et al. (2011):

$$D' = 10^{-5}(0.15T - 1.9). \quad \text{(B10)}$$

The water vapor diffusivity, corrected for kinetic effects, is (Grabowski et al. 2011):

$$D = D'\left[\frac{r_i}{r_i + \Delta_c} + \frac{D'}{r_i \alpha_c}\left(\frac{2\pi}{R_d T}\right)^{1/2}\right]^{-1}, \quad \text{(B11)}$$

with accommodation coefficient $\alpha_c = 0.036$ and jump length for water vapor $\Delta_c = 0.104$ μm (Pruppacher and Klett 1997, their Table 13.1).

Thermal conductivity K' (W m^{-1} K^{-1}, excluding kinetic effects) is taken from Grabowski et al. (2011):

$$K' = 1.5^{-11}T^3 - 4.8 \times 10^{-8}T^2 + 10^{-4}T - 3.9 \times 10^{-4}. \quad \text{(B12)}$$

Accounting for kinetic effects, the thermal conductivity K is given by Grabowski et al. [2011, their Eq. (11b)]:

$$K = K'\left[\frac{r_i}{r_i + \Delta_T} + \frac{K'}{r_i \alpha_T \rho_a c_p}\left(\frac{2\pi}{R_d T}\right)^{1/2}\right]^{-1}, \quad \text{(B13)}$$

with accommodation coefficient $\alpha_T = 0.7$ and jump length for heat $\Delta_T = 0.216$ μm (Pruppacher and Klett 1997, their Table 13.1).

The equilibrium saturation ratio S_{eq}, accounting for curvature and solute effects, is

$$S_{eq} = \exp\left[\frac{2\sigma_w}{R_v \rho_w T r_i} - \frac{\mathscr{V}\Phi_s m_{si}\frac{M_w}{M_s}}{\frac{4\pi}{3}\rho_w(r_i^3 - r_{di}^3)}\right]. \quad \text{(B14)}$$

Based on Pruppacher and Klett (1997), the molality of a solution drop can be written as

$$\mathscr{M} = \frac{m_{si}}{M_s \rho_w\left(\frac{4\pi}{3}r_i^3 - \frac{m_{si}}{\rho_s}\right)}. \quad \text{(B15)}$$

The practical osmotic coefficient Φ_s as a function of molality is interpolated from the values in Robinson and Stokes (1959) for NaCl.

The model is initialized by assuming that drops formed on aerosol particles are in equilibrium with the ambient humidity, typically about 300 m below cloud base. For the condensation-only runs, Eqs. (B1)–(B5) are integrated using a fourth-order Runge–Kutta routine up to cloud top and subsequently down to cloud base. On the descending branch, the calculations are stopped at the same altitude where the parcel was initially exactly saturated on ascent (the cloud-base altitude).

In the following, let subscript i refer to small and j to large drop size classes. For the cases where gravitational coalescence is allowed (larger drops capturing smaller drops), the drop growth equation for the large drop size class is given by

$$\frac{dr_j}{dt} = \left.\frac{dr_j}{dt}\right|_{\text{condensation}} + \left.\frac{dr_j}{dt}\right|_{\text{coalescence}}, \quad \text{(B16)}$$

where the condensation term for drop class j is given by Eq. (B1), and the coalescence term is given by

$$\left.\frac{dr_j}{dt}\right|_{\text{coalescence}} = \sum_{i=1}^{j-1}\pi(r_j + r_i)^2(v_{tj} - v_{ti})E(r_i, r_j)\frac{r_i^3}{3r_j^2}N_i. \quad \text{(B17)}$$

Here, collision efficiencies are from Pinsky et al. (2001), and terminal velocities are calculated from Beard (1976).

To account for removal of smaller drops by capture of larger drops, the concentration of smaller drops is changed:

$$\left.\frac{N_i}{dt}\right|_{\text{coalescence}} = \sum_{j=i+1}^{J}\pi(r_j + r_i)^2(v_{tj} - v_{ti})E(r_j, r_i)N_j N_i, \quad \text{(B18)}$$

where J is the total number of drop classes.

Thus, for the runs with both condensation and coalescence, Eqs. (B1)–(B5) and (B16)–(B18) are integrated using a fourth-order Runge–Kutta routine.

REFERENCES

Albrecht, B. A., 1989: Aerosols, cloud microphysics, and fractional cloudiness. *Science*, **245**, 1227–1230, doi:10.1126/science.245.4923.1227.

Andrejczuk, M., J. M. Reisner, B. Henson, M. K. Dubey, and C. A. Jeffery, 2008: The potential impact of pollution on a nondrizzling stratus deck: Does aerosol number matter more than aerosol type? *J. Geophys. Res.*, **113**, D19204, doi:10.1029/2007JD009445.

——, W. W. Grabowski, J. Reisner, and A. Gadian, 2010: Cloud–aerosol interactions for boundary layer stratocumulus in the Lagrangian Cloud Model. *J. Geophys. Res.*, **115**, D22214, doi:10.1029/2010JD014248.

Baker, M. B., and J. Latham, 1979: The evolution of droplet spectra and the production of embryonic raindrops in small cumulus clouds. *J. Atmos. Sci.*, **36**, 1612–1615, doi:10.1175/1520-0469(1979)036<1612:TEODSA>2.0.CO;2.

Beard, K. V., 1976: Terminal velocity and shape of cloud and precipitation drops aloft. *J. Atmos. Sci.*, **33**, 851–864, doi:10.1175/1520-0469(1976)033<0851:TVASOC>2.0.CO;2.

Blot, R., and Coauthors, 2013: Ultrafine sea spray aerosol over the southeastern Pacific: Open-ocean contributions to marine boundary layer CCN. *Atmos. Chem. Phys.*, **13**, 7263–7278, doi:10.5194/acp-13-7263-2013.

Blyth, A. M., S. G. Lasher-Trapp, W. A. Cooper, C. A. Knight, and J. Latham, 2003: The role of giant and ultragiant nuclei in the formation of early radar echoes in warm cumulus clouds. *J. Atmos. Sci.*, **60**, 2557–2572, doi:10.1175/1520-0469(2003)060<2557:TROGAU>2.0.CO;2.

Bolton, D., 1980: The computation of equivalent potential temperature. *Mon. Wea. Rev.*, **108**, 1046–1053, doi:10.1175/1520-0493(1980)108<1046:TCOEPT>2.0.CO;2.

Bott, A., 2001: A new method for the solution of the stochastic collection equation in cloud models with spectral aerosol and cloud drop microphysics. *Atmos. Res.*, **59–60**, 361–372, doi:10.1016/S0169-8095(01)00125-9.

Cooper, W. A., R. T. Bruintjes, and G. K. Mather, 1997: Calculations pertaining to hygroscopic seeding with flares. *J. Appl. Meteor.*, **36**, 1449–1469, doi:10.1175/1520-0450(1997)036<1449:CPTHSW>2.0.CO;2.

——, S. G. Lasher-Trapp, and A. M. Blyth, 2013: The influence of entrainment and mixing on the initial formation of rain in a warm cumulus cloud. *J. Atmos. Sci.*, **70**, 1727–1743, doi:10.1175/JAS-D-12-0128.1.

Cui, Z., A. Gadian, A. Blyth, J. Crosier, and I. Crawford, 2014: Observations of the variation in aerosol and cloud microphysical properties along the 20°S transect on 13 November 2008 during VOCALS-REx. *J. Atmos. Sci.*, **71**, 2927–2943, doi:10.1175/JAS-D-13-0245.1.

Eastman, R., S. G. Warren, and C. J. Hahn, 2011: Variations in cloud cover and cloud types over the ocean from surface observations, 1954–2008. *J. Climate*, **24**, 5914–5934, doi:10.1175/2011JCLI3972.1.

Feingold, G., S. M. Kreidenweiss, B. Stevens, and W. R. Cotton, 1996: Numerical simulations of stratocumulus processing of cloud condensation nuclei through collision-coalescence. *J. Geophys. Res.*, **101**, 21 391–21 402, doi:10.1029/96JD01552.

——, W. R. Cotton, S. M. Kreidenweis, and J. T. Davis, 1999: The impact of giant cloud condensation nuclei on drizzle formation in stratocumulus: Implications for cloud radiative properties. *J. Atmos. Sci.*, **56**, 4100–4117, doi:10.1175/1520-0469(1999)056<4100:TIOGCC>2.0.CO;2.

Fountikis, C., and A. Nenes, 2005: Continued development of a cloud droplet formation parameterization for global climate models. *J. Geophys. Res.*, **110**, D11212, doi:10.1029/2004JD005591.

Franklin, C. N., P. A. Villaincourt, M. K. Yau, and P. Bartello, 2005: Collision rates of cloud droplets in turbulent flow. *J. Atmos. Sci.*, **62**, 2451–2466, doi:10.1175/JAS3493.1.

Grabowski, W. W., M. Andrejczuk, and L.-P. Wang, 2011: Droplet growth in a bin warm-rain scheme with Twomey CCN activation. *Atmos. Res.*, **99**, 290–311, doi:10.1016/j.atmosres.2010.10.020.

Gras, J. L., and G. P. Ayers, 1983: Marine aerosol at southern mid-latitudes. *J. Geophys. Res.*, **88**, 10 661–10 666, doi:10.1029/JC088iC15p10661.

Howell, W. E., 1949: The growth of cloud drops in uniformly cooled air. *J. Meteor.*, **6**, 134–149, doi:10.1175/1520-0469(1949)006<0134:TGOCDI>2.0.CO;2.

IPCC, 2013: *Climate Change 2013: The Physical Science Basis.* Cambridge University Press, 1535 pp., doi:10.1017/CBO9781107415324.

Ivanova, E. T., Ye. L. Kogan, I. P. Mazin, and M. S. Permyakov, 1977: Method of parameterizing the condensation process of droplet growth in numerical cloud models. *Izv., Atmos. Oceanic Phys.*, **13**, 821–826.

Jensen, J. B., and S. Lee, 2008: Giant sea-salt aerosols and warm rain formation in marine stratocumulus. *J. Atmos. Sci.*, **65**, 3678–3694, doi:10.1175/2008JAS2617.1.

——, ——, P. B. Krummel, and D. Gogoasa, 2000: Precipitation in marine stratocumulus. Part I: Thermodynamic and dynamic observations of closed cell circulations and cumulus bands. *Atmos. Res.*, **54**, 117–155, doi:10.1016/S0169-8095(00)00040-5.

Johnson, D. B., 1982: The role of giant and ultragiant nuclei in warm rain initiation. *J. Atmos. Sci.*, **39**, 448–460, doi:10.1175/1520-0469(1982)039<0448:TROGAU>2.0.CO;2.

Jonas, P. R., 1996: Turbulence and cloud microphysics. *Atmos. Res.*, **40**, 283–306, doi:10.1016/0169-8095(95)00035-6.

Keith, C. H., and A. B. Arons, 1954: The growth of sea-salt particles by condensation of atmospheric water vapor. *J. Meteor.*, **11**, 173–184, doi:10.1175/1520-0469(1954)011<0173:TGOSSP>2.0.CO;2.

Khairoutdinov, M. F., and Y. L. Kogan, 1999: A large-eddy simulation model with explicit microphysics: Validation against aircraft observations of a stratocumulus-topped boundary layer. *J. Atmos. Sci.*, **56**, 2115–2131, doi:10.1175/1520-0469(1999)056<2115:ALESMW>2.0.CO;2.

——, and ——, 2000: A new cloud physics parameterization in a large-eddy simulation model of marine stratocumulus. *J. Atmos. Sci.*, **128**, 229–243, doi:10.1175/1520-0493(2000)128<0229:ANCPPI>2.0.CO;2.

Kogan, Y. L., 1991: The simulation of a convective cloud in a 3-D model with explicit microphysics. Part I: Model description and sensitivity analysis. *J. Atmos. Sci.*, **48**, 1160–1189, doi:10.1175/1520-0469(1991)048<1160:TSOACC>2.0.CO;2.

——, D. B. Mechem, and K. Choi, 2012: Effects of sea-salt aerosols on precipitation in simulations of shallow cumulus. *J. Atmos. Sci.*, **69**, 463–483, doi:10.1175/JAS-D-11-031.1.

Kulmala, M., A. Laaksonen, R. J. Charlson, and P. Korhonen, 1997: Clouds without supersaturation. *Nature*, **388**, 336–337, doi:10.1038/41000.

Lasher-Trapp, S. G., W. A. Cooper, and A. M. Blyth, 2002: Measurements of ultragiant aerosol particles in the atmosphere from the small cumulus microphysics study. *J. Atmos. Oceanic Technol.*, **19**, 402–408, doi:10.1175/1520-0426(2002)019<0402:MOUAPI>2.0.CO;2.

——, ——, and ——, 2005: Broadening of the droplet size distribution from entrainment and mixing in a cumulus cloud. *Quart. J. Roy. Meteor. Soc.*, **131**, 195–220, doi:10.1256/qj.03.199.

Lebo, Z. J., and J. H. Seinfeld, 2011: A continuous spectral aerosol-droplet microphysics model. *Atmos. Chem. Phys.*, **11**, 12 297–12 316, doi:10.5194/acp-11-12297-2011.

——, N. C. Johnson, and J. Y. Harrington, 2008: Radiative influences on ice crystal and droplet growth within mixed-phase stratus clouds. *J. Geophys. Res.*, **113**, doi:10.1029/2007JD009262.

Lewis, E. R., and S. E. Schwartz, 2004: *Sea Salt Aerosol Production: Mechanisms, Methods, Measurements, and Models—A Critical*

Review. Geophys. Monogr., Vol. 152, Amer. Geophys. Union, 413 pp., doi:10.1029/GM152.

Lin, Y.-L., R. D. Farley, and H. D. Orville, 1983: Bulk parameterization of the snow field in a cloud model. *J. Climate Appl. Meteor.*, **22**, 1065–1092, doi:10.1175/1520-0450(1983)022<1065: BPOTSF>2.0.CO;2.

Liu, Y., P. H. Daum, R. McGraw, and R. Wood, 2006: Parameterization of the autoconversion process. Part II: Generalization of Sundqvist-type parameterizations. *J. Atmos. Sci.*, **63**, 1103–1109, doi:10.1175/JAS3675.1.

Lothon, M., D. H. Lenschow, D. Leon, and G. Vali, 2005: Turbulence measurements in marine stratocumulus with airborne Doppler radar. *Quart. J. Roy. Meteor. Soc.*, **131**, 2063–2080, doi:10.1256/qj.04.131.

Lowenstein, J. H., A. M. Blyth, and R. P. Lawson, 2010: Early evolution of the largest-sized droplets in maritime cumulus clouds. *Quart. J. Roy. Meteor. Soc.*, **136**, 708–717, doi:10.1002/qj.597.

Magaritz, L., M. Pinksy, O. Krasnov, and A. Khain, 2009: Investigation of droplet size distributions and drizzle formation using a new trajectory ensemble model. Part II: Lucky parcels. *J. Atmos. Sci.*, **66**, 781–805, doi:10.1175/2008JAS2789.1.

Martin, G. M., D. W. Johnson, and A. Spice, 1994: The measurement and parameterization of effective radius of droplets in warm stratocumulus clouds. *J. Atmos. Sci.*, **51**, 1823–1842, doi:10.1175/1520-0469(1994)051<1823:TMAPOE>2.0.CO;2.

Mordy, W., 1959: Computations of the growth by condensation of a population of cloud drops. *Tellus*, **11**, 16–44, doi:10.1111/j.2153-3490.1959.tb00003.x.

Morrison, H., J. A. Curry, and V. I. Khvorostyanov, 2005: A new double-moment microphysics parameterization for application in cloud and climate models. Part I: Description. *J. Atmos. Sci.*, **62**, 1665–1677, doi:10.1175/JAS3446.1.

Novakov, T., and J. E. Penner, 1993: Large contribution of organic aerosols to cloud-condensation-nuclei concentrations. *Nature*, **365**, 823–826, doi:10.1038/365823a0.

Pinsky, M., A. Khain, and M. Shapiro, 2001: Collision efficiency of drops in a wide range of Reynolds numbers: Effects of pressure on spectrum evolution. *J. Atmos. Sci.*, **58**, 742–764, doi:10.1175/1520-0469(2001)058<0742:CEODIA>2.0.CO;2.

Posselt, R., and U. Lohmann, 2008: Influence of giant CCN on warm rain processes. *Atmos. Chem. Phys.*, **8**, 3769–3788, doi:10.5194/acp-8-3769-2008.

Pruppacher, H. R., and J. D. Klett, 1997: *Microphysics of Clouds and Precipitation*. 2nd ed. Springer, 954 pp.

Rauber, R. M., and Coauthors, 2007: Rain in shallow cumulus over the ocean: The RICO campaign. *Bull. Amer. Meteor. Soc.*, **88**, 1912–1928, doi:10.1175/BAMS-88-12-1912.

Reiche, C. H., and S. Lasher-Trapp, 2010: The minor importance of giant aerosol to precipitation development within small trade wind cumuli observed during RICO. *Atmos. Res.*, **95**, 386–399, doi:10.1016/j.atmosres.2009.11.002.

Roach, W. T., 1976: On the effect of radiative exchange on the growth by condensation of a cloud or fog droplet. *Quart. J. Roy. Meteor. Soc.*, **102**, 361–372, doi:10.1002/qj.49710243207.

Robinson, R. A., and R. H. Stokes, 1959: *Electrolyte Solutions*. 3rd ed. Butterworths, 571 pp.

Rogers, R. R., and M. K. Yau, 1989: *A Short Course in Cloud Physics*. Pergamon Press, 293 pp.

Rosenfeld, D., and I. M. Lensky, 1998: Satellite-based insight into precipitation formation processes in continental and maritime convective clouds. *Bull. Amer. Meteor. Soc.*, **79**, 2457–2476, doi:10.1175/1520-0477(1998)079<2457:SBIIPF>2.0.CO;2.

Segal, Y., A. Khain, M. Pinsky, and D. Rosenfeld, 2004: Effects of hygroscopic seeding on raindrop formation as seen from simulations using a 2000-bin spectral cloud parcel model. *Atmos. Res.*, **71**, 3–34, doi:10.1016/j.atmosres.2004.03.003.

Shima, S., K. Kusano, A. Kawano, T. Sugiyama, and S. Kawahara, 2009: The super-droplet method for the numerical simulation of clouds and precipitation: A particle-based and probabilistic microphysics model coupled with a non-hydrostatic model. *Quart. J. Roy. Meteor. Soc.*, **135**, 1307–1320, doi:10.1002/qj.441.

Tang, I. N., A. C. Tridico, and K. H. Fung, 1997: Thermodynamic and optical properties of sea salt aerosols. *J. Geophys. Res.*, **102**, 23 269–23 275, doi:10.1029/97JD01806.

Telford, J. W., 1955: A new aspect of condensation theory. *J. Meteor.*, **12**, 436–444, doi:10.1175/1520-0469(1955)012<0436: ANAOCT>2.0.CO;2.

Thompson, G., and T. Eidhammer, 2014: A study of aerosol impacts on clouds and precipitation development in a large winter cyclone. *J. Atmos. Sci.*, **71**, 3636–3658, doi:10.1175/JAS-D-13-0305.1.

Twohy, C. H., and Coauthors, 2013: Impacts of aerosol particles on the microphysical and radiative properties of stratocumulus clouds over the southeast Pacific Ocean. *Atmos. Chem. Phys.*, **13**, 2541–2562, doi:10.5194/acp-13-2541-2013.

Twomey, S., 1977: The influence of pollution on the shortwave albedo of clouds. *J. Atmos. Sci.*, **34**, 1149–1152, doi:10.1175/1520-0469(1977)034<1149:TIOPOT>2.0.CO;2.

Tzivion, S., G. Feingold, and Z. Levin, 1987: An efficient numerical solution to the stochastic collection equation. *J. Atmos. Sci.*, **44**, 2139–2149, doi:10.1175/1520-0469(1987)044<3139: AENSTT>2.0.CO;2.

Wang, L.-P., Y. Xue, O. Ayala, and W. W. Grabowski, 2006: Effects of stochastic coalescence and air turbulence on the size distribution of cloud droplets. *Atmos. Res.*, **82**, 416–432, doi:10.1016/j.atmosres.2005.12.011.

Wood, R., 2005: Drizzle in stratiform boundary layer clouds. Part II: Microphysical aspects. *J. Atmos. Sci.*, **62**, 3034–3050, doi:10.1175/JAS3530.1.

——, and Coauthors, 2011: The VAMOS Ocean–Cloud–Atmosphere–Land Study Regional Experiment (VOCALS-Rex): Goals, platforms, and field operations. *Atmos. Chem. Phys.*, **11**, 627–654, doi:10.5194/acp-11-627-2011.

Woodcock, A. H., 1953: Salt nuclei in marine air as a function of altitude and wind force. *J. Meteor.*, **10**, 362–371, doi:10.1175/1520-0469(1953)010<0366:SNIMAA>2.0.CO;2.